Joint Relational Database Generation via Graph-Conditional Diffusion Models

Mohamed Amine Ketata, David Lüdke, Leo Schwinn, Stephan Günnemann

School of Computation, Information and Technology & Munich Data Science Institute
Technical University of Munich, Germany
Correspondence to: a.ketata@tum.de

Abstract

Building generative models for relational databases (RDBs) is important for applications like privacy-preserving data release and augmenting real datasets. However, most prior work either focuses on single-table generation or relies on autoregressive factorizations that impose a fixed table order and generate tables sequentially. This approach limits parallelism, restricts flexibility in downstream applications like missing value imputation, and compounds errors due to commonly made conditional independence assumptions. We propose a fundamentally different approach: jointly modeling all tables in an RDB without imposing any order. By using a natural graph representation of RDBs, we propose the Graph-Conditional Relational Diffusion Model (GRDM). GRDM leverages a graph neural network to jointly denoise row attributes and capture complex inter-table dependencies. Extensive experiments on six real-world RDBs demonstrate that our approach substantially outperforms autoregressive baselines in modeling multi-hop inter-table correlations and achieves state-of-the-art performance on single-table fidelity metrics.

1 Introduction

Relational databases (RDBs), which organize data into multiple interlinked tables, are the most widely used data management system, estimated to store over 70% of the world's structured data [1]. RDBs are used in different domains such as healthcare, finance, education, and e-commerce [2, 3]. However, increasing legal and ethical concerns around data privacy have led to strict regulations that limit access to data containing personal or sensitive information. While these safeguards protect the privacy of individuals and organizations, they can hinder the development of data-driven technologies that benefit from rich, structured data, thereby slowing scientific progress.

Synthetic data generation has emerged as a promising approach to mitigate this problem by training generative models on private datasets and releasing synthetic samples that preserve key statistical prop-

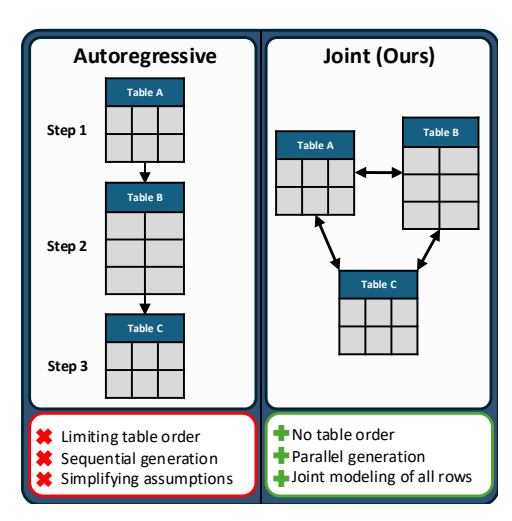


Figure 1: Comparison of autoregressive and joint relational database generation.

erties without disclosing sensitive information [4, 5]. In addition to enabling privacy-preserving data sharing, synthetic data can improve fairness, support data augmentation, and facilitate robust downstream analysis [6, 7].

Despite recent advances in synthetic data generation for single-table settings [8–12], *multi-table* relational database generation remains underexplored, and current approaches share a common limitation: they impose a fixed order on the tables and model their distribution autoregressively [13–16] (*cf.* Figure 1 left). This sequential generation procedure introduces several key limitations. It constrains downstream tasks such as missing data imputation, prevents parallel sampling, and often struggles with capturing complex long-range dependencies between tables. In addition, prior methods often adopt strong conditional independence assumptions that facilitate learning but sacrifice fidelity or generality [15].

In this paper, we propose a fundamentally different approach: we jointly model all tables in a relational database without relying on a specific table ordering (cf. Figure 1 right) and propose the first non-autoregressive generative model for RDBs. To achieve this, we adopt a graph-based representation of RDBs [17], where nodes correspond to individual rows, and edges encode primary-foreign key relationships. By framing RDB generation as a graph generation problem, we leverage random graph generation methods to first sample a graph that preserves node degree distributions of the real graph, then jointly generate all node features using our novel Graph-Conditional Relational Diffusion Model (GRDM). Our main contributions are the following:

- We introduce a new framework that models the joint distribution over all tables in an RDB, removing the need for a predefined table ordering or autoregressive factorization.
- We propose GRDM, the first non-autoregressive generative model for RDBs. It uses a graph-based representation and jointly generates all row attributes.
- We demonstrate that GRDM significantly outperforms autoregressive baselines across six real-world RDBs, especially in capturing long-range dependencies between tables.

2 Background

Relational Databases. A *Relational Database* (RDB) [18] $(\mathcal{R}, \mathcal{L})$ (cf. Figure 2 top) is defined by a set of m interconnected tables, called relations, $\mathcal{R} = \{R^{(1)}, \dots, R^{(m)}\}$ and a database schema $\mathcal{L} \subseteq \mathcal{R} \times \mathcal{R}$ that specifies the connections between them. Specifically, a tuple (R_{child}, R_{parent}) belongs to \mathcal{L} if rows from R_{child} contain references to rows from R_{parent} , forming a parent-child relationship. Each table $R^{(i)}$ represents one entity type and consists of n_i rows $\{r_1^{(i)}, \dots, r_{n_i}^{(i)}\}$, where each row r is an instance of this entity and consists of three components [17]:

- **Primary key** p_r : a unique identifier for each row within a table.
- Foreign keys $\mathcal{K}_r \subseteq \{p_{r'} \mid r' \in R' \text{ and } (R, R') \in \mathcal{L}\}$: a set of primary keys of rows in other tables, that row r points to. We refer to these rows as r's parents.
- Attributes x_r : a set of *columns* (features) describing this specific instance. In this work, we focus on databases with categorical and numerical attributes, which include ordinal, date, time, discrete, and continuous data.

Synthetic Relational Database Generation. The goal of synthetic RDB generation is to learn a parameterized distribution $p_{\theta} \approx p(\mathcal{R})$ to sample a synthetic database $\tilde{\mathcal{R}}$ that adheres to the schema \mathcal{L} and preserves the statistical properties of \mathcal{R} . The challenges of this learning problem are twofold:

- (i) the complex distributions of columns with heterogeneous multi-modal features (column shapes),
- (ii) the complex correlations between columns from the same table (intra-table trends), as well as columns from different tables (inter-table trends) which can be directly (one-hop) or indirectly (multi-hop) connected by primary-foreign key links.

Autoregressive Models for RDB Generation. To learn these distributions and capture their correlations, existing generative models for RDBs rely on a specific table order, often the topological order induced by the schema \mathcal{L} , to autoregressively factorize the joint distribution [13, 16, 15, 19, 14]:

$$p(\mathcal{R}) = p(R^{(1)}, \dots, R^{(m)}) = \prod_{i=1}^{m} p(R^{(i)} \mid \{R^{(i')} \mid i' < i\}).^{1}$$

¹Some works [16, 19] generate all primary and foreign keys in a first step, then apply a similar autoregressive factorization on the attributes (non-key columns).

While this factorization can, in principle, model the true joint distribution, its inherent sequential nature introduces two key limitations. First, *fixing the table order* limits downstream applications, e.g., missing value imputation, because each table is conditioned only on its predecessors and cannot incorporate information from tables later in the order. Second, the factorization forces the *generation runtime* to scale linearly with the number of tables and prevents parallelization across tables.

Moreover, learning the required conditional probability distributions is practically challenging, particularly for large RDBs with high-dimensional attributes and complex *multi-hop* inter-table dependencies. To make the problem tractable, prior work focused on RDBs with only two tables [16] or resorted to simplifying assumptions such as Markov-like conditional independence assumptions of tables or individual rows given their parents [13–15]. Such assumptions are particularly problematic in this autoregressive setting, where small errors can accumulate across generation steps, causing compounding errors and loss of coherence.

3 Joint Modeling of All Tables with Graph-Conditional Diffusion Models

In this work, we introduce the first non-autoregressive generative model for RDBs by directly modeling the *joint* distribution of tables in \mathcal{R} . Specifically, by avoiding any table ordering and leveraging the relational structure of the database to jointly model its rows, our approach imposes fewer assumptions and enables models that are more expressive, flexible, and parallelizable. We structure this section as follows: we introduce how to faithfully model RDBs as graphs in Section 3.1, motivate our two-step graph generation procedure in Section 3.2, describe how we generate the graph structure in Section 3.3, and finally present our novel diffusion model, which is the main contribution of this paper, in Section 3.4.

3.1 Relational Databases as Attributed Heterogeneous Directed Graphs

The relational structure of an RDB is naturally represented as a directed heterogeneous graph that elegantly models its different components. A key advantage of adopting this graph-based view is that we can leverage the vast literature on graph theory and graph machine learning to process relational data. This idea has gained traction in recent representation learning work [20, 17, 21], and has also been explored in generative modeling [16, 19], though existing approaches remain autoregressive. While there are several ways to represent an RDB as a graph [21], we adopt the simple and intuitive formulation from Fey et al. [17], modeling an RDB (\mathcal{R}, \mathcal{L}) as a heterogeneous graph in which each row is a node and edges are defined by primary–foreign key links (cf. Figure 2 bottom).

Formally, we define the graph as $\mathcal{G}=(\mathcal{V},\mathcal{E},\mathcal{X})$, with node set \mathcal{V} representing the rows, edge set \mathcal{E} representing the primary–foreign key connections, and feature set \mathcal{X} representing the attributes. First, we map each row $r\in R^{(i)}$ to a node v of type i, resulting in a heterogeneous graph. The full node set is given by $\mathcal{V}=\bigcup_{i=1}^m \mathcal{V}^{(i)}$, where each $\mathcal{V}^{(i)}=\{v(r)\mid r\in R^{(i)}\}$ contains all nodes of type i and v(r) denotes the node corresponding to row r, and r(v) its inverse. Second, we define the edge set as

$$\mathcal{E} = \{ (v_1, v_2) \in \mathcal{V} \times \mathcal{V} \mid p_{v_2} \in \mathcal{K}_{v_1} \},$$

where $p_v=p_{r(v)}$ and $\mathcal{K}_v=\mathcal{K}_{r(v)}$ are shorthand for accessing a node's primary and foreign keys.

Each edge represents a primary-foreign key relationship between two rows. We assign each edge a type (i,j), based on the types of its endpoints v_1 and v_2 . Since edges are ordered pairs, the resulting graph is directed—a property that is essential for reconstructing the original RDB from its graph representation. Finally, the feature set is defined as $\mathcal{X} = \{x_v \mid v \in \mathcal{V}\}$, where $x_v = x_{r(v)}$ contains the non-key attributes of the corresponding row. Thus,

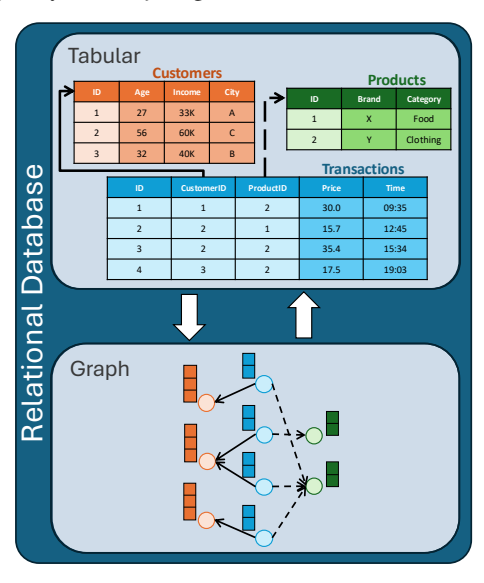


Figure 2: Tabular and graph representations of relational databases. We use different colours and different arrow shapes to depict different node and edge types, respectively.

 \mathcal{X} captures all columns in \mathcal{R} that are not primary or foreign keys, while the primary and foreign keys are fully encoded in the (featureless) graph structure $(\mathcal{V}, \mathcal{E})$.

Importantly, this graph construction is a *faithful* representation of the original RDB in the sense that one can reconstruct the original RDB \mathcal{R} from the graph \mathcal{G} – up to permutations of the primary keys (thus also of foreign keys). One concrete procedure for this reconstruction is provided in Appendix B.1. In the following, we use \mathcal{G} and \mathcal{R} interchangeably to refer to the graph and RDB representation of the same object. With this, our target data distribution becomes:

$$p(\mathcal{R}) = p(\mathcal{G}) = p(\mathcal{V}, \mathcal{E}, \mathcal{X}). \tag{1}$$

3.2 On the Factorization of $p(V, \mathcal{E}, \mathcal{X})$

To find an efficient and scalable parametrization for $p(\mathcal{V}, \mathcal{E}, \mathcal{X})$, we examine its possible factorizations. First, note that \mathcal{V} is implicitly defined by either \mathcal{X} or \mathcal{E} . Hence, we can reduce the problem to three viable factorizations: (A) one-shot; $p(\mathcal{V}, \mathcal{E}, \mathcal{X})$, (B) features-then-edges; $p(\mathcal{V}, \mathcal{X})p(\mathcal{E}|\mathcal{V}, \mathcal{X})$, or (C) edges-then-features; $p(\mathcal{V}, \mathcal{E})p(\mathcal{X}|\mathcal{V}, \mathcal{E})$.

To illustrate the scalability trade-offs among these factorizations, consider an RDB with two tables containing n and m rows, respectively. Note that for factorizations (A) and (B), the edges are generated along with or after the features identifying each node. Thus, they need to consider all $n \times m$ possible edges, which is computationally prohibitive for large n and m, and increasingly so for databases with multiple tables. In contrast, factorization (C) generates the edges before the features, which allows us to sidestep this combinatorial explosion by exploiting the exchangeability of nodes and simply parameterizing the number of nodes and their per edge-type degree for efficient random graph generation similar to Xu et al. [16]. Specifically, factorizing the distribution as

$$p(\mathcal{R}) = p(\mathcal{G}) = p(\mathcal{V}, \mathcal{E})p(\mathcal{X}|\mathcal{V}, \mathcal{E})$$
(2)

corresponds to a two-step process. First, $p(\mathcal{V}, \mathcal{E})$ defines the structure of the attribute-free graph, equivalent to generating the primary and foreign key columns of the RDB. Second, $p(\mathcal{X}|\mathcal{V}, \mathcal{E})$ generates the node features of the graph, or equivalently, the row attributes of the RDB. Note that this can be attained by jointly modeling each node with its neighborhood defined by the graph structure, allowing us to scale to very large databases. In the following, we build up on this factorization: Section 3.3 presents a simple and effective algorithm for modeling $p(\mathcal{V}, \mathcal{E})$, followed by our main contribution, a graph-conditional diffusion framework for modeling $p(\mathcal{X}|\mathcal{V}, \mathcal{E})$, in Section 3.4.

3.3 Node Degree-Preserving Random Graph Generation

The featureless graph $(\mathcal{V}, \mathcal{E})$ is a directed, heterogeneous, and m-partite graph—edges exist only between nodes of different types, corresponding to rows from different tables. We model $p(\mathcal{V}, \mathcal{E})$ using a simple random graph generation algorithm that preserves the node degree distributions observed in the real graph [22]. We define a node's *indegree* and *outdegree* for a given edge type as the number of incoming and outgoing edges of that type, respectively. Outdegrees are constant per edge type, since each table has a fixed number of foreign key columns. Thus, our goal is to preserve the indegree distribution for each edge type.

The learning phase computes the empirical indegree distributions per edge type from the real graph. Sampling begins with root nodes—those with no outgoing edges. We set the number of root nodes to match the real graph, ensuring a similar overall graph size, but the graph size can also be scaled by a multiplier. For each root node, we sample its children according to the learned indegree distributions and recursively repeat this process for the sampled child nodes. When a node has multiple parents, this procedure initially produces multiple copies for it. To correct this while preserving the overall indegree distribution, we perform a random matching to merge duplicate nodes across these sets, before sampling their indegree sequence.

3.4 Graph-Conditional Relational Diffusion Model (GRDM)

Given the graph structure $(\mathcal{V}, \mathcal{E})$, we are now interested in generating the features \mathcal{X} . Since this is now a feature generation task for a fixed graph structure, an interesting analogy to keep in mind is image generation. An image can be viewed as a graph with a simple 2D grid structure, where each pixel represents a node with a 3-dimensional feature vector of color channels. In our case, we can think

about $p(\mathcal{X}|\mathcal{V},\mathcal{E})$ as generating a very large image, with a more complex structure and heterogeneous node features. Inspired by the success of diffusion models in image generation and other domains [23–26], and given their unprecedented capacity to model joint distributions, we propose to model $p(\mathcal{X}|\mathcal{V},\mathcal{E})$ using diffusion models. Our model can be viewed as a generalization of image diffusion models to graphs with arbitrary structures and node features. In this section, we use $\mathcal{X}^{(0)}$ to denote the original data \mathcal{X} , as is common in the diffusion models literature [23].

3.4.1 Forward Process

Diffusion models [27, 23] are latent variable models that define a sequence of latent variables $\mathcal{X}^{(1)}, \dots, \mathcal{X}^{(T)}$ of the same dimensionality as $\mathcal{X}^{(0)}$ through a fixed Markov chain, called the *forward process* or *diffusion process*, that gradually adds noise to data:

$$q(\mathcal{X}^{(1:T)}|\mathcal{X}^{(0)}, \mathcal{V}, \mathcal{E}) = \prod_{t=1}^{T} q(\mathcal{X}^{(t)}|\mathcal{X}^{(t-1)}, \mathcal{V}, \mathcal{E}).$$
(3)

While this formulation is very general and allows defining complex forward processes, we choose to add noise *independently* to all nodes at each timestep t (analogous to how pixels are independently noised in image diffusion models), which will enable efficient training of our model:

$$q(\mathcal{X}^{(t)}|\mathcal{X}^{(t-1)}, \mathcal{V}, \mathcal{E}) = \prod_{v \in \mathcal{V}} q(\boldsymbol{x}_v^{(t)}|\boldsymbol{x}_v^{(t-1)}), \tag{4}$$

where $\boldsymbol{x}_v^{(t)}$ is the feature vector of node v at diffusion timestep t. In this work, we assume that \boldsymbol{x}_v consists of numerical and categorical features. A common way to model categorical tabular data is multinomial diffusion [28, 8], however, it suffers significant performance overheads and we found it unstable for high-cardinality categorical variables. Therefore, we follow Pang et al. [15] and map categorical variables to continuous space through label encoding (See Appendix B.2 for details) and apply Gaussian diffusion (DDPM [23]) on the unified space: $q(\boldsymbol{x}_v^{(t)}|\boldsymbol{x}_v^{(t-1)}) = \mathcal{N}(\boldsymbol{x}_v^{(t)}; \sqrt{1-\beta_t}\boldsymbol{x}_v^{(t-1)}, \beta_t \boldsymbol{I})$, where β_1, \dots, β_T define the variance schedule.

An important consequence of this choice of the forward process, i.e., adding *Gaussian* noise *independently* to all nodes, is that we can sample $\boldsymbol{x}_v^{(t)}$ of an individual node at any timestep t directly from the clean data at time 0, which is key for efficient training of the model. Let $\alpha_t = 1 - \beta_t$ and $\bar{\alpha}_t = \prod_{i=1}^t \alpha_i$, then $q(\boldsymbol{x}_v^{(t)}|\mathcal{X}^{(0)}, \mathcal{V}, \mathcal{E}) = q(\boldsymbol{x}_v^{(t)}|\boldsymbol{x}_v^{(0)}) = \mathcal{N}(\boldsymbol{x}_v^{(t)}; \sqrt{\bar{\alpha}_t}\boldsymbol{x}_v^{(0)}, (1 - \bar{\alpha}_t)\boldsymbol{I})$.

3.4.2 Reverse Process

The generative model is defined as another Markov chain with learned transitions; the reverse process,

$$p_{\theta}(\mathcal{X}^{(0:T)}|\mathcal{V},\mathcal{E}) = p(\mathcal{X}^{(T)}|\mathcal{V},\mathcal{E}) \prod_{t=1}^{T} p_{\theta}(\mathcal{X}^{(t-1)}|\mathcal{X}^{(t)},\mathcal{V},\mathcal{E}).$$
 (5)

This formulation of the reverse process also offers significant modeling flexibility; to predict the less noisy state $x_v^{(t-1)}$ of node v, the model can leverage the graph structure $(\mathcal{V}, \mathcal{E})$ and the features of all other nodes $\mathcal{X}^{(t)}$. However, doing so is not scalable for large graphs, but also not necessary because most of the nodes will be irrelevant. Therefore, we propose to condition the denoising of node v at each timestep on the local neighborhood encoding the relations of the database, which achieves our goal of jointly modeling the nodes faithfully to the RDB structure. This is analogous to how convolutional neural network-based image diffusion models condition the denoising of a pixel on its neighboring pixels [23].

To allow a node to interact not only with its parents, but also with its children, for the diffusion model, we treat the graph $\mathcal G$ as undirected by adding reverse edges to all existing edges in $\mathcal G$. Formally, let $\mathcal G_{v,K}^{(t)}=(\mathcal V_{v,K},\mathcal E_{v,K},\mathcal X_{v,K}^{(t)})$ denote the subgraph from $\mathcal G$ (now undirected), centered at node v, containing all nodes in the K-hop neighborhood around v, with features at diffusion time t. For instance, for K=1, the nodes in $\mathcal G_{v,1}^{(t)}$ correspond to all rows in the database that are referenced by r(v) and those that reference it. Note that we can also bound the worst-case space and time

complexity by sampling a fixed-size set of neighbors as proposed by Hamilton et al. [29]. Formally, we model the following factorization of the reverse process (Equation 5):

$$p(\mathcal{X}^{(T)}|\mathcal{V},\mathcal{E}) = \prod_{v \in \mathcal{V}} p(\boldsymbol{x}_v^{(T)}) \text{ and } p_{\theta}(\mathcal{X}^{(t-1)}|\mathcal{X}^{(t)},\mathcal{V},\mathcal{E}) = \prod_{v \in \mathcal{V}} p_{\theta}(\boldsymbol{x}_v^{(t-1)}|\mathcal{G}_{v,K}^{(t)}). \tag{6}$$

A crucial property of our reverse process formulation is the following: due to the multi-step nature of diffusion models, the denoising of node v is not restricted to only conditioning on its K-hop neighborhood, but can extend to further away nodes. To see this, let us consider two consecutive timesteps and identify which nodes in $\mathcal{X}^{(t+1)}$ influence $\boldsymbol{x}^{(t-1)}_v$. From Equation 6, we see that from $t \to t-1$, only nodes in $\mathcal{X}^{(t)}_{v,K}$ influence $\boldsymbol{x}^{(t-1)}_v$. However, from $t+1 \to t$, all nodes in $\mathcal{X}^{(t)}_{v,K}$ are in turn influenced by nodes in their respective K-hop neighborhood at time t+1, which will indirectly influence $\boldsymbol{x}^{(t-1)}_v$. These nodes form the subgraph $\mathcal{G}^{(t+1)}_{v,2K}$, and by induction on the number of diffusion steps, we can show that $\boldsymbol{x}^{(t)}_v$ is influenced by $\mathcal{G}^{(t+N)}_{v,NK}$ at time t+N, meaning that our model can in principle model interactions between node pairs that are $\mathcal{O}(TK)$ hops away in the graph during the whole reverse diffusion process. Empirically, this is shown by the model using K=1 and is able to capture higher-order correlations well (See Section 4 for detailed experiments).

In the case of Gaussian diffusion, the reverse process is also Gaussian: $p(\boldsymbol{x}_v^{(T)}) = \mathcal{N}(\boldsymbol{x}_v^{(T)}; \boldsymbol{0}, \boldsymbol{I})$ and $p_{\theta}(\boldsymbol{x}_v^{(t-1)}|\mathcal{G}_{v,K}^{(t)}) = \mathcal{N}(\boldsymbol{x}_v^{(t-1)}; \boldsymbol{\mu}_{\theta}(\mathcal{G}_{v,K}^{(t)}, t), \sigma_t^2 \boldsymbol{I})$, where $\boldsymbol{\mu}_{\theta}$ is a neural network that learns to approximate the less noisy state of node v given its neighborhood at time t, and σ_t is a hyperparameter.

3.4.3 Training and Sampling

Training. Recall that our end goal is to learn a parametrized model p_{θ} for the distribution $p(\mathcal{X}^{(0)}|\mathcal{V},\mathcal{E})$. p_{θ} can be learned by minimizing the model's negative log-likelihood (NLL) of the data, $-\log p_{\theta}(\mathcal{X}^{(0)}|\mathcal{V},\mathcal{E})$. However, the NLL is intractable to compute; we therefore optimize its variational bound [27]:

$$-\log p_{\theta}(\mathcal{X}^{(0)}|\mathcal{V},\mathcal{E}) \leq \mathbb{E}_{q} \left[-\log \frac{p_{\theta}(\mathcal{X}^{(0:T)}|\mathcal{V},\mathcal{E})}{q(\mathcal{X}^{(1:T)}|\mathcal{X}^{(0)},\mathcal{V},\mathcal{E})} \right] =: L(\theta). \tag{7}$$

 $L(\theta)$ can be equivalently expressed in terms of conditional forward process posteriors, which are tractable to compute (see Appendix A for a detailed derivation). Furthermore, we follow Ho et al. [23] in parametrizing μ_{θ} as $\mu_{\theta}(\mathcal{G}_{v,K}^{(t)},t)=\frac{1}{\sqrt{\alpha_{t}}}\left(\boldsymbol{x}_{v}^{(t)}-\frac{\beta_{t}}{\sqrt{1-\bar{\alpha}_{t}}}\boldsymbol{\epsilon}_{\theta}(\mathcal{G}_{v,K}^{(t)},t)\right)$, where $\boldsymbol{\epsilon}_{\theta}$ predicts the noise added at time t, and using a simplified training objective (details are provided in Appendix A), leading to the following objective that we use to train our model:

$$L_{\text{simple}}(\theta) = \mathbb{E}_{v \sim U(\mathcal{V}), t \sim U(\{1, \dots, T\}), \{\epsilon_{v'} \sim \mathcal{N}(\mathbf{0}, \mathbf{I}) \mid v' \in \mathcal{V}_{v, K}\}} \left[\left\| \epsilon_v - \epsilon_{\theta} \left(\mathcal{G}_{v, K}^{(t)}, t \right) \right\|^2 \right], \quad (8)$$

where U samples an element from its input set uniformly at random. Our model, ϵ_{θ} , is trained by minimizing $L_{\text{simple}}(\theta)$ using stochastic gradient descent, where each iteration works as follows: a node v is sampled uniformly at random and is noised along with its K-hop neighborhood to the *same* time step t, which is also sampled uniformly at random. Given the noisy subgraph $\mathcal{G}_{v,K}^{(t)}$, ϵ_{θ} learns to predict the noise vector ϵ_v that was added to v. Algorithm 1 shows the detailed training procedure.

Sampling. To sample from our model, we initialize all node features in the graph with Gaussian noise, $\boldsymbol{x}_v^{(T)} \sim \mathcal{N}(\boldsymbol{0}, \boldsymbol{I}) \ \forall \ v \in \mathcal{V}$. Then, at each time step $t = T, \dots, 1$, all nodes are jointly denoised before moving to the next step as follows:

$$\boldsymbol{x}_{v}^{(t-1)} = \frac{1}{\sqrt{\alpha_{t}}} \left(\boldsymbol{x}_{v}^{(t)} - \frac{\beta_{t}}{\sqrt{1 - \bar{\alpha}_{t}}} \boldsymbol{\epsilon}_{\theta} \left(\mathcal{G}_{v,K}^{(t)}, t \right) \right) + \sigma_{t} \boldsymbol{z}_{v} \ \forall \ v \in \mathcal{V}, \tag{9}$$

where $z_v \sim \mathcal{N}(0, I)$ if t > 1 else $z_v = 0$. The full sampling procedure is shown in Algorithm 2.

A nice property of our sampling procedure is that at each time step, the denoising step (Equation 9) can be run fully in parallel across all nodes in the graph, allowing us to scale to very large graphs. This is in contrast to prior works [15, 19] that specify an order on the tables and can only start with generating one table, once all its predecessors have been generated.

3.4.4 Model architecture

 ϵ_{θ} is a learnable function that maps a graph \mathcal{G} centered at node v and a timestep t to a vector of the same dimension as x_v , denoted as d. Formally, $\epsilon_{\theta}: \mathbb{G} \times \mathbb{R} \to \mathbb{R}^d$, where \mathbb{G} is the set of graphs.

In this work, we use heterogeneous Message-Passing Graph Neural Networks (MP-GNNs) [30, 31] to parameterize ϵ_{θ} . Let $(\mathcal{G},t) \in \mathbb{G} \times \mathbb{R}$ denote the input to ϵ_{θ} with $\mathcal{G} = (\mathcal{V}, \mathcal{E}, \mathcal{X})$. We define initial node embeddings as $\mathbf{h}_v^0 = (\mathbf{x}_v, t) \ \forall \ v \in \mathcal{V}$. One iteration of heterogeneous message passing consists of updating each node's embedding at iteration l, \mathbf{h}_v^l , based on its neighbors, to get updated embeddings \mathbf{h}_v^{l+1} , where nodes and edges of different types are treated differently. In Appendix B.4, we present a general formulation of heterogeneous MP-GNNs. In this work, we use the heterogeneous version of the GraphSAGE model [29, 32] with sum-based neighbor aggregation.

After L iterations of message passing, we obtain a set of deep node embeddings $\{h_v^L\}_{v\in\mathcal{V}}$. We set L to be the same as the number of hops K used to select $\mathcal{G}_{v,K}$. Finally, to predict the noise vector $\hat{\epsilon}_v$ for the target node v, we further pass the final embedding of node v through a multi-layer perceptron (MLP) [33]: $\hat{\epsilon}_v = \text{MLP}(\boldsymbol{h}_v^L)$, which is the final output of ϵ_θ .

4 Experiments

In this section, we evaluate our model's performance in synthetic relational database generation, using both single-table and multi-table fidelity metrics, including long-range dependency metrics introduced in [15]. We present a detailed comparison of our model to different state-of-the-art baselines on six real-world databases, followed by a more detailed analysis and an ablation study for our model.

4.1 Experimental Setup

Real-world Databases. We use six real-world relational databases in our experiments. Five were used in the evaluation setup in [15]: *Berka* [34], *Instacart 05* [35], *Movie Lens* [36, 37], *CCS* [36], and *California* [38]. In addition, we use the *RelBench-F1* database [39] from RelBench [40], a recently introduced benchmark for relational deep learning [17]. We chose *F1* because it contains nine tables—more than any of the previous five RDBs—and includes a relatively high number of numerical and categorical columns, compared to other databases in RelBench. The used databases vary in the number of tables, size, maximum depth, number of inter-table connections, and feature complexity. We provide more details on these databases in Appendix C.1. Note that *Berka*, *Instacart 05*, and *RelBench-F1* exhibit the most complex inter-table correlations with up to 3-hop interactions.

Baselines. We compare our model to four relational database generation methods from the literature. \underline{SDV} [13] is a statistical method tailored for RDB synthesis based on Gaussian Copulas. $\underline{ClavaDDPM}$ [15] is a state-of-the-art diffusion-based model that leverages cluster labels and classifier-guided diffusion models to generate a child table conditioned on its parent. In addition, we adopt two synthesis pipelines used by Pang et al. [15] to provide additional insights: SingleTable and \underline{Denorm} . SingleTable generates foreign keys based on the real group size distribution, i.e., the distribution of row counts that have the same foreign key, similarly to our random graph generation algorithm. However, it learns and generates each table individually and independently of all other tables. It can be seen as a version of our model with the number of hops K set to 0. Denorm is based on the idea of joining tables first, so it learns and generates the joined table of every connected pair, and then splits it. For both these baselines, we use the same DDPM-based tabular diffusion backbone as our model [23, 8]. For all DDPM-based baselines, we use the exact same hyperparameters for model architecture and training as our model for a fair comparison. For SDV, we used the default hyperparameters as in [15]. More implementation details are provided in Appendix C.2.

Evaluation Metrics. To evaluate the quality of the synthetic data in terms of fidelity, we follow [15] and report the following metrics implemented in the SDMetrics package [41]. 1) *Cardinality* compares the distribution of the number of children rows that each parent row has, between the real and synthetic data. We compute this metric for each parent-child pair and report the average across all pairs. 2) *Column Shapes* compares the marginal distributions of individual columns between the real and synthetic data. We compute this metric for every column of each table and report their average. 3) *Intra-Table Trends* measures the correlation between a pair of columns in the same table

Table 1: Comparison of the Fidelity metrics described in Section 4.1. The best method in each metric is highlighted, and we report the relative improvement of GRDM compared to the closest baseline. Databases are ordered by complexity. SDV does not support RDBs with more than 5 tables.

	SDV	SingleTable	Denorm	ClavaDDPM	GRDM (Ours)	Improvement (%)
Berka	1					
CARDINALITY		97.06 ± 0.80	$96.06 {\scriptstyle~\pm 1.15}$	$96.75 \scriptstyle~\pm 0.26$	99.70 ± 0.07	+2.72
COLUMN SHAPES		94.58 ± 0.01	83.28 ± 0.97	$94.60{\scriptstyle~\pm0.41}$	96.90 ± 0.07	+2.43
INTRA-TABLE TRENDS	> 5 tables	$91.72{\scriptstyle~\pm 0.23}$	$72.12{\scriptstyle~\pm0.73}$	$90.53{\scriptstyle~\pm 1.93}$	98.21 ± 0.05	+7.08
INTER-TABLE TRENDS (1-HOP)	> 5 tables	$81.77{\scriptstyle~\pm 1.19}$	$55.77{\scriptstyle~\pm2.80}$	$83.79{\scriptstyle~\pm4.21}$	92.94 ± 0.06	+10.92
INTER-TABLE TRENDS (2-HOP)		$78.09{\scriptstyle~\pm0.53}$	$57.68{\scriptstyle~\pm1.67}$	$85.87 \scriptstyle~\pm 2.72$	96.04 ± 0.20	+11.84
INTER-TABLE TRENDS (3-HOP)		$75.56{\scriptstyle~\pm 0.34}$	$55.59{\scriptstyle~\pm1.48}$	80.98 ± 3.12	93.13 ± 0.47	+15.00
Instacart 05						
CARDINALITY		$94.73{\scriptstyle~\pm0.14}$	94.98 ± 0.84	$94.91{\scriptstyle~\pm 1.50}$	99.96 ± 0.01	+5.24
COLUMN SHAPES		89.30 ± 0.00	$71.83{\scriptstyle~\pm 0.32}$	90.18 ± 0.43	98.87 ± 0.06	+9.64
INTRA-TABLE TRENDS	> 5 tables	99.70 ± 0.00	88.74 ± 0.00	99.68 ± 0.02	98.33 ± 0.04	-1.37
INTER-TABLE TRENDS (1-HOP)		66.93 ± 0.07	62.58 ± 0.05	75.84 ± 0.36	92.03 ± 0.30	+21.35
INTER-TABLE TRENDS (2-HOP)		$16.22{\scriptstyle~\pm13.41}$	$0.00~\pm0.00$	$14.40{\scriptstyle~\pm20.37}$	$96.17 \scriptstyle~\pm 0.15$	+492.91
RelBench-F1						
CARDINALITY		$94.94 \scriptstyle~\pm 1.06$	$93.39{\scriptstyle~\pm1.56}$	$94.04{\scriptstyle~\pm2.33}$	98.26 ± 0.12	+3.50
COLUMN SHAPES		$95.93{\scriptstyle~\pm0.16}$	$89.25{\scriptstyle~\pm 0.28}$	95.19 ± 0.75	97.28 ± 0.29	+1.41
INTRA-TABLE TRENDS	> 5 tables	$95.80{\scriptstyle~\pm0.29}$	90.30 ± 0.56	$94.71{\scriptstyle~\pm0.63}$	96.74 ± 0.36	+0.98
INTER-TABLE TRENDS (1-HOP)		$79.61{\scriptstyle~\pm0.65}$	$65.60{\scriptstyle~\pm0.45}$	88.19 ± 0.27	93.74 ± 0.50	+6.29
INTER-TABLE TRENDS (2-HOP)		$74.10{\scriptstyle~\pm2.71}$	$62.21{\scriptstyle~\pm0.38}$	$83.17{\scriptstyle~\pm 1.39}$	$96.81{\scriptstyle~\pm0.28}$	+16.40
Movie Lens						
CARDINALITY		98.99 ± 0.16	98.87 ± 0.26	$98.79{\scriptstyle~\pm0.13}$	98.80 ± 0.36	-0.19
COLUMN SHAPES	> 5 tables	99.19 ± 0.00	$78.03{\scriptstyle~\pm0.17}$	99.11 ± 0.09	98.22 ± 0.05	-0.98
INTRA-TABLE TRENDS	> 5 tables	98.56 ± 0.01	57.33 ± 0.10	$98.52{\scriptstyle~\pm0.05}$	96.24 ± 0.24	-2.35
INTER-TABLE TRENDS (1-HOP)		$92.72{\scriptstyle~\pm 0.09}$	$77.45{\scriptstyle~\pm 1.93}$	$92.11{\scriptstyle~\pm2.12}$	95.60 ± 0.17	+3.11
CCS						
CARDINALITY	$74.36 {\scriptstyle~\pm8.40}$	$99.37{\scriptstyle~\pm0.16}$	$26.70{\scriptstyle~\pm 0.20}$	98.96 ± 0.79	99.79 ± 0.03	+0.42
COLUMN SHAPES	69.04 ± 4.38	$95.20{\scriptstyle~\pm0.00}$	$79.29{\scriptstyle~\pm0.13}$	92.64 ± 3.93	97.03 ± 0.37	+1.92
INTRA-TABLE TRENDS	94.84 ± 1.00	98.96 ± 0.00	86.60 ± 0.14	$97.75{\scriptstyle~\pm1.70}$	93.60 ± 2.61	-5.42
INTER-TABLE TRENDS (1-HOP)	21.74 ± 9.62	$51.62{\scriptstyle~\pm0.22}$	57.77 ± 0.69	$72.65{\scriptstyle~\pm8.10}$	85.54 ± 2.91	+17.74
California						
CARDINALITY	71.45 ± 0.00	$99.89{\scriptstyle~\pm0.04}$	99.87 ± 0.02	$98.99{\scriptstyle~\pm0.69}$	99.96 ± 0.01	+0.07
COLUMN SHAPES	72.32 ± 0.00	$99.51{\scriptstyle~\pm0.04}$	94.99 ± 0.02	98.76 ± 0.27	99.15 ± 0.02	-0.36
INTRA-TABLE TRENDS	50.23 ± 0.00	98.69 ± 0.08	$94.17 \scriptstyle~\pm 0.01$	$97.65{\scriptstyle~\pm0.39}$	98.00 ± 0.01	-0.70
INTER-TABLE TRENDS (1-HOP)	54.89 ± 0.00	$92.96 \scriptstyle~\pm 0.05$	$87.24{\scriptstyle~\pm0.10}$	$95.34{\scriptstyle~\pm0.48}$	97.68 ± 0.01	+2.45

and computes the similarity in correlation between the real and synthetic data. We report the average across all column pairs of each table. 4) *Inter-Table Trends* (k-hop) is similar to the previous metric but measures the correlation between column pairs from tables at distance k, e.g., 1-hop for columns from parent-child pairs. For each possible $k \geq 1$, we report the average across all column pairs that are k hops away from each other. This is the most challenging and most interesting metric because it considers interactions between different tables.

For each of these metrics, we use the Kolmogorov-Smirnov (KS) statistic and the Total Variation (TV) distance to compare distributions of numerical and categorical values, respectively. To compare correlations of columns pairs, we use the Pearson correlation coefficient for numerical values and the contingency table for categorical values. All metrics are normalized to lie between 0 (least fidelity) and 100 (highest fidelity). Detailed descriptions of these metric computations are in Appendix C.3.

4.2 Evaluation Results

Table 1 reports the fidelity metrics described in Section 4.1 across six databases for all methods, including standard deviations over three random seeds. **GRDM consistently outperforms all base-lines on Inter-Table Trends across all databases**, particularly in capturing multi-hop correlations for the most complex RDBs. On *Berka*, which has the most complex schema with up to 3-hop dependencies, GRDM surpasses the best baseline by 15% on 3-hop correlations and 11.84% on 2-hop correlations. On *Instacart 05* and *RelBench-F1*, GRDM improves over the best baseline by more than 5 times and 16.4% on 2-hop correlations, respectively. For 1-hop correlations, GRDM achieves an average gain of 10.31% over all databases. These improvements highlight the effectiveness of our joint modeling approach over the autoregressive methods used by other baselines (with the exception of Single-Table, which treats tables independently). On single-table metrics, GRDM performs comparably to the best methods and even outperforms them on certain databases.

4.3 Ablation Study

Our experiments are primarily designed to assess the impact of jointly modeling all tables in an RDB versus learning an autoregressive factorization. To ensure a fair comparison, we used the same hyperparameters across all datasets and all diffusion-based methods, including the diffusion backbone and training settings. The GNN component is unique to our model; we adopted its configuration from [17], which uses fewer parameters than the diffusion guidance classifiers in [15]. We conducted an ablation study to understand the impact of major design decisions, focusing on two core com-

Table 2: Ablation study on the three most complex RDBs. We compare our default setting from Table 1 with K=1 and with a sequential version of our model.

	K = 2 (Default)	K = 1	K=1, Sequential
Berka			
CARDINALITY	99.70 ± 0.07	99.70 ± 0.07	99.70 ± 0.07
COLUMN SHAPES	96.90 ±0.07	97.18 ± 0.03	38.97 ± 3.65
INTRA-TABLE TRENDS	98.21 ±0.05	98.47 ± 0.07	52.10 ± 2.98
INTER-TABLE TRENDS (1-HOP)	92.94 ± 0.06	93.21 ± 0.04	28.53 ± 3.84
INTER-TABLE TRENDS (2-HOP)	96.04 ± 0.20	95.69 ± 0.19	52.01 ± 2.55
INTER-TABLE TRENDS (3-HOP)	93.13 ± 0.47	$92.84 \scriptstyle~\pm 0.14$	$49.45{\scriptstyle~\pm4.14}$
Instacart 05	1		
CARDINALITY	99.96 ± 0.01	99.96 ± 0.01	99.96 ± 0.01
COLUMN SHAPES	98.87 ± 0.06	98.40 ± 0.01	67.51 ± 3.93
INTRA-TABLE TRENDS	98.33 ± 0.04	97.53 ± 0.06	89.33 ± 2.27
INTER-TABLE TRENDS (1-HOP)	92.03 ± 0.30	88.83 ± 0.70	63.32 ± 2.01
INTER-TABLE TRENDS (2-HOP)	96.17 ± 0.15	93.30 ± 0.08	$13.41{\scriptstyle~\pm3.64}$
RelBench-F1	1		
CARDINALITY	98.26 ± 0.12	98.26 ± 0.12	98.26 ± 0.12
COLUMN SHAPES	97.28 ± 0.29	96.76 ± 0.06	94.83 ± 0.09
INTRA-TABLE TRENDS	96.74 ± 0.36	95.92 ± 0.04	95.01 ±0.75
INTER-TABLE TRENDS (1-HOP)	93.74 ± 0.50	93.33 ± 0.17	90.82 ±0.37
INTER-TABLE TRENDS (2-HOP)	$96.81{\scriptstyle~\pm0.28}$	96.33 ± 0.08	87.73 ± 0.86

ponents: the number of hops K, and the joint modeling aspect (see Table 2). We report results on the three databases with the most complex schema, *Berka*, *Instacart 05*, and *RelBench-F1*, in Table 2.

Effect of the number of hops K. The first two columns in Table 2 compare the metrics of K=2 with K=1. While K=2 yields slightly better results, the K=1 variant still outperforms all baselines on multi-hop correlation metrics (cf. Table 1), which highlights that long-range dependencies can be effectively captured through diffusion, as a node's receptive field increases with each diffusion step (see Section 3.4.2 for a detailed discussion). Note that K=1 offers better computational efficiency than K=2; on Berka, K=1 was 25% faster than K=2 in generating the RDB.

Effect of joint modeling. To isolate the impact of our joint modeling approach, we implemented an autoregressive variant of our model that retains all other components (e.g., graph representation, GNN architecture). Instead of modeling $p(\mathcal{X}|\mathcal{V},\mathcal{E})$ directly, it factorizes the distribution as $\prod_{i=1}^m p(\mathcal{X}^{(i)} \mid \{\mathcal{X}^{(i')} \mid i' < i\})$, where $\mathcal{X}^{(i)}$ denotes features of node type i. As shown in Table 2, this version performs significantly worse, not only on inter-table correlations, but also on single-table metrics. This aligns with observations from [15], who introduced latent cluster variables to mitigate the difficulty of learning conditional distributions with noisy and high-dimensional conditing space. Note that the sequential generation is significantly slower than the joint model. Concretely, on Berka, the autoregressive model was more than 2.5 times slower than its joint counterpart (both with K=1).

5 Conclusion

We introduced GRDM, the first non-autoregressive generative model for RDBs. GRDM represents RDBs as graphs by mapping rows to nodes and primary–foreign key links to edges. It first generates a graph structure using a degree-preserving random graph model, then jointly generates all node features—i.e., row attributes—via a novel diffusion model that conditions each node's denoising on its K-hop neighborhood. This enables modeling long-range dependencies due to the iterative nature of diffusion models. GRDM consistently outperformed baselines on six real-world RDBs, particularly in capturing long-range correlations.

Limitations and Future Work. This work lays the foundation for scalable and expressive generative models for RDBs, and opens several avenues for future research. First, while our graph generation method is simple and effective, more tailored approaches could better capture the structure of relational data. Second, although we use a straightforward graph representation, alternatives—such as modeling certain tables (e.g., transactions or reviews) as attributed edges—may be more appropriate for specific tasks. Third, while this work focuses on unconditional generation, GRDM can be extended to support downstream tasks and serve as a foundational model for relational data. Finally, equipping GRDM with differential privacy guarantees could further increase its practical adoption, especially in sensitive domains.

Acknowledgments

This project was funded by SAP SE. It is also supported by the DAAD programme Konrad Zuse Schools of Excellence in Artificial Intelligence, sponsored by the Federal Ministry of Education and Research. We thank Pedro Henrique Martins, Maximilian Schambach, Sirine Ayadi, and Tim Beyer for their valuable feedback.

References

- [1] DB-Engines. DBMS popularity broken down by database model, 2023. Available: https://db-engines.com/en/ranking_categories.
- [2] Alistair EW Johnson, Tom J Pollard, Lu Shen, Li-wei H Lehman, Mengling Feng, Mohammad Ghassemi, Benjamin Moody, Peter Szolovits, Leo Anthony Celi, and Roger G Mark. Mimic-iii, a freely accessible critical care database. *Scientific data*, 3(1):1–9, 2016.
- [3] PubMed. National Center for Biotechnology Information, U.S. National Library of Medicine, 1996. Available: https://www.ncbi.nlm.nih.gov/pubmed/.
- [4] Aldren Gonzales, Guruprabha Guruswamy, and Scott R Smith. Synthetic data in health care: A narrative review. *PLOS Digital Health*, 2(1):e0000082, 2023.
- [5] Vamsi K Potluru, Daniel Borrajo, Andrea Coletta, Niccolò Dalmasso, Yousef El-Laham, Elizabeth Fons, Mohsen Ghassemi, Sriram Gopalakrishnan, Vikesh Gosai, Eleonora Kreačić, et al. Synthetic data applications in finance. *arXiv preprint arXiv:2401.00081*, 2023.
- [6] Joao Fonseca and Fernando Bacao. Tabular and latent space synthetic data generation: a literature review. *Journal of Big Data*, 10(1):115, 2023.
- [7] Boris Van Breugel and Mihaela Van der Schaar. Beyond privacy: Navigating the opportunities and challenges of synthetic data. *arXiv preprint arXiv:2304.03722*, 2023.
- [8] Akim Kotelnikov, Dmitry Baranchuk, Ivan Rubachev, and Artem Babenko. Tabddpm: Modelling tabular data with diffusion models. In *International Conference on Machine Learning*, pages 17564–17579. PMLR, 2023.
- [9] Tennison Liu, Zhaozhi Qian, Jeroen Berrevoets, and Mihaela van der Schaar. Goggle: Generative modelling for tabular data by learning relational structure. In *The Eleventh International Conference on Learning Representations*, 2023.
- [10] Hengrui Zhang, Jiani Zhang, Balasubramaniam Srinivasan, Zhengyuan Shen, Xiao Qin, Christos Faloutsos, Huzefa Rangwala, and George Karypis. Mixed-type tabular data synthesis with score-based diffusion in latent space. *arXiv preprint arXiv:2310.09656*, 2023.
- [11] Juntong Shi, Minkai Xu, Harper Hua, Hengrui Zhang, Stefano Ermon, and Jure Leskovec. Tabdiff: a multi-modal diffusion model for tabular data generation. *arXiv preprint arXiv:2410.20626*, 2024.
- [12] Xi Fang, Weijie Xu, Fiona Anting Tan, Jiani Zhang, Ziqing Hu, Yanjun Qi, Scott Nickleach, Diego Socolinsky, Srinivasan Sengamedu, and Christos Faloutsos. Large language models (llms) on tabular data: Prediction, generation, and understanding—a survey. arXiv preprint arXiv:2402.17944, 2024.
- [13] Neha Patki, Roy Wedge, and Kalyan Veeramachaneni. The synthetic data vault. In 2016 IEEE international conference on data science and advanced analytics (DSAA), pages 399–410. IEEE, 2016.
- [14] Kuntai Cai, Xiaokui Xiao, and Graham Cormode. Privlava: synthesizing relational data with foreign keys under differential privacy. *Proceedings of the ACM on Management of Data*, 1(2): 1–25, 2023.
- [15] Wei Pang, Masoumeh Shafieinejad, Lucy Liu, Stephanie Hazlewood, and Xi He. Clavaddpm: Multi-relational data synthesis with cluster-guided diffusion models. Advances in Neural Information Processing Systems, 37:83521–83547, 2024.

- [16] Kai Xu, Georgi Ganev, Emile Joubert, Rees Davison, Olivier Van Acker, and Luke Robinson. Synthetic data generation of many-to-many datasets via random graph generation. In *The Eleventh International Conference on Learning Representations*, 2022.
- [17] Matthias Fey, Weihua Hu, Kexin Huang, Jan Eric Lenssen, Rishabh Ranjan, Joshua Robinson, Rex Ying, Jiaxuan You, and Jure Leskovec. Relational deep learning: Graph representation learning on relational databases. *arXiv preprint arXiv:2312.04615*, 2023.
- [18] Edgar F Codd. A relational model of data for large shared data banks. *Communications of the ACM*, 13(6):377–387, 1970.
- [19] Valter Hudovernik. Relational data generation with graph neural networks and latent diffusion models. In NeurIPS 2024 Third Table Representation Learning Workshop, 2024.
- [20] Lukáš Zahradník, Jan Neumann, and Gustav Šír. A deep learning blueprint for relational databases. In *NeurIPS 2023 Second Table Representation Learning Workshop*, 2023.
- [21] Minjie Wang, Quan Gan, David Wipf, Zhenkun Cai, Ning Li, Jianheng Tang, Yanlin Zhang, Zizhao Zhang, Zunyao Mao, Yakun Song, et al. 4dbinfer: A 4d benchmarking toolbox for graph-centric predictive modeling on relational dbs. *arXiv* preprint arXiv:2404.18209, 2024.
- [22] Michael Molloy and Bruce Reed. A critical point for random graphs with a given degree sequence. *Random structures & algorithms*, 6(2-3):161–180, 1995.
- [23] Jonathan Ho, Ajay Jain, and Pieter Abbeel. Denoising diffusion probabilistic models. *Advances in neural information processing systems*, 33:6840–6851, 2020.
- [24] Prafulla Dhariwal and Alexander Nichol. Diffusion models beat gans on image synthesis. *Advances in neural information processing systems*, 34:8780–8794, 2021.
- [25] Chitwan Saharia, William Chan, Saurabh Saxena, Lala Li, Jay Whang, Emily L Denton, Kamyar Ghasemipour, Raphael Gontijo Lopes, Burcu Karagol Ayan, Tim Salimans, et al. Photorealistic text-to-image diffusion models with deep language understanding. Advances in neural information processing systems, 35:36479–36494, 2022.
- [26] Aaron Lou, Chenlin Meng, and Stefano Ermon. Discrete diffusion modeling by estimating the ratios of the data distribution. *arXiv preprint arXiv:2310.16834*, 2023.
- [27] Jascha Sohl-Dickstein, Eric Weiss, Niru Maheswaranathan, and Surya Ganguli. Deep unsupervised learning using nonequilibrium thermodynamics. In *International conference on machine* learning, pages 2256–2265. pmlr, 2015.
- [28] Emiel Hoogeboom, Didrik Nielsen, Priyank Jaini, Patrick Forré, and Max Welling. Argmax flows and multinomial diffusion: Learning categorical distributions. *Advances in neural information processing systems*, 34:12454–12465, 2021.
- [29] Will Hamilton, Zhitao Ying, and Jure Leskovec. Inductive representation learning on large graphs. *Advances in neural information processing systems*, 30, 2017.
- [30] Justin Gilmer, Samuel S Schoenholz, Patrick F Riley, Oriol Vinyals, and George E Dahl. Neural message passing for quantum chemistry. In *International conference on machine learning*, pages 1263–1272. PMLR, 2017.
- [31] Michael Schlichtkrull, Thomas N Kipf, Peter Bloem, Rianne Van Den Berg, Ivan Titov, and Max Welling. Modeling relational data with graph convolutional networks. In *The semantic web: 15th international conference, ESWC 2018, Heraklion, Crete, Greece, June 3–7, 2018, proceedings 15*, pages 593–607. Springer, 2018.
- [32] Matthias Fey and Jan Eric Lenssen. Fast graph representation learning with pytorch geometric. *arXiv preprint arXiv:1903.02428*, 2019.
- [33] Yury Gorishniy, Ivan Rubachev, Valentin Khrulkov, and Artem Babenko. Revisiting deep learning models for tabular data. *Advances in neural information processing systems*, 34: 18932–18943, 2021.

- [34] Petr Berka et al. Guide to the financial data set. PKDD2000 discovery challenge, 2000.
- [35] jeremy stanley, Meg Risdal, sharathrao, and Will Cukierski. Instacart market basket analysis, 2017. URL https://kaggle.com/competitions/instacart-market-basket-analysis.
- [36] Jan Motl and Oliver Schulte. The ctu prague relational learning repository. *arXiv preprint* arXiv:1511.03086, 2015.
- [37] Oliver Schulte, Zhensong Qian, Arthur E Kirkpatrick, Xiaoqian Yin, and Yan Sun. Fast learning of relational dependency networks. *Machine Learning*, 103:377–406, 2016.
- [38] MP Center. Integrated public use microdata series, international: Version 7.3 [data set]. minneapolis, mn: Ipums, 2020.
- [39] Open source formula 1 database, 2025. URL https://github.com/f1db/f1db.
- [40] Joshua Robinson, Rishabh Ranjan, Weihua Hu, Kexin Huang, Jiaqi Han, Alejandro Dobles, Matthias Fey, Jan Eric Lenssen, Yiwen Yuan, Zecheng Zhang, et al. Relbench: A benchmark for deep learning on relational databases. *Advances in Neural Information Processing Systems*, 37:21330–21341, 2024.
- [41] Synthetic Data Metrics. DataCebo, Inc., 12 2024. URL https://docs.sdv.dev/sdmetrics/. Version 0.18.0.

A Detailed Loss Derivation

We provide a detailed derivation for the NLL loss following [27, 23]. For notation brevity, we drop the conditioning on V, E in the following:

$$\begin{split} &-\log p_{\theta}(\mathcal{X}^{(0)}) \\ &\leq \mathbb{E}_{q} \left[-\log \frac{p_{\theta}(\mathcal{X}^{(0:T)})}{q(\mathcal{X}^{(1:T)}|\mathcal{X}^{(0)})} \right] \\ &= \mathbb{E}_{q} \left[-\log p(\mathcal{X}^{(T)}) - \sum_{t=1}^{T} \log \frac{p_{\theta}(\mathcal{X}^{(t-1)}|\mathcal{X}^{(t)})}{q(\mathcal{X}^{(t)}|\mathcal{X}^{(t-1)})} \right] \\ &= \mathbb{E}_{q} \left[-\log p(x_{v}^{(T)}) - \sum_{t=1}^{T} \sum_{v \in \mathcal{V}} \log \frac{p_{\theta}(x_{v}^{(t-1)}|\mathcal{G}_{v,K}^{(t)})}{q(x_{v}^{(t)}|x_{v}^{(t-1)})} \right] \\ &= \mathbb{E}_{q} \left[-\sum_{v \in \mathcal{V}} \log p(x_{v}^{(T)}) - \sum_{t=2}^{T} \sum_{v \in \mathcal{V}} \log \frac{p_{\theta}(x_{v}^{(t-1)}|\mathcal{G}_{v,K}^{(t)})}{q(x_{v}^{(t-1)}|x_{v}^{(t)},x_{v}^{(0)})} - \sum_{v \in \mathcal{V}} \log \frac{p_{\theta}(x_{v}^{(0)}|\mathcal{G}_{v,K}^{(1)})}{q(x_{v}^{(t-1)}|x_{v}^{(t)},x_{v}^{(0)})} \cdot \frac{q(x_{v}^{(t-1)}|x_{v}^{(0)})}{q(x_{v}^{(t)}|x_{v}^{(0)})} \right] \\ &= \mathbb{E}_{q} \left[-\sum_{v \in \mathcal{V}} \log p(x_{v}^{(T)}) - \sum_{t=2}^{T} \sum_{v \in \mathcal{V}} \log \frac{p_{\theta}(x_{v}^{(t-1)}|\mathcal{G}_{v,K}^{(t)})}{q(x_{v}^{(t)}|x_{v}^{(0)})} - \sum_{v \in \mathcal{V}} \log \frac{p_{\theta}(x_{v}^{(t-1)}|x_{v}^{(t)},x_{v}^{(0)})}{q(x_{v}^{(t-1)}|x_{v}^{(t)},x_{v}^{(0)})} - \sum_{v \in \mathcal{V}} \log p_{\theta}(x_{v}^{(0)}|\mathcal{G}_{v,K}^{(1)}) \right] \\ &= \mathbb{E}_{q} \left[-\sum_{v \in \mathcal{V}} \log \frac{p(x_{v}^{(T)})}{q(x_{v}^{(T)}|x_{v}^{(0)})} - \sum_{t=2}^{T} \sum_{v \in \mathcal{V}} \log \frac{p_{\theta}(x_{v}^{(t-1)}|\mathcal{G}_{v,K}^{(t)})}{q(x_{v}^{(t-1)}|x_{v}^{(t)},x_{v}^{(0)})} - \sum_{v \in \mathcal{V}} \log p_{\theta}(x_{v}^{(0)}|\mathcal{G}_{v,K}^{(1)}) \right] \\ &= \mathbb{E}_{q} \left[\sum_{v \in \mathcal{V}} \underbrace{D_{KL} \left(q(x_{v}^{(T)}|x_{v}^{(v)}) \| p(x_{v}^{(T)}) \right)}_{L_{v}^{(T)}} + \sum_{t=2}^{T} \sum_{v \in \mathcal{V}} \underbrace{D_{KL} \left(q(x_{v}^{(t-1)}|x_{v}^{(t)},x_{v}^{(0)}) \| p_{\theta}(x_{v}^{(t-1)}|\mathcal{G}_{v,K}^{(t)})} \right)}_{L_{v}^{(t-1)}} - \sum_{v \in \mathcal{V}} \underbrace{D_{KL} \left(q(x_{v}^{(t-1)}|x_{v}^{(t)},x_{v}^{(0)}) \| p_{\theta}(x_{v}^{(t-1)}|\mathcal{G}_{v,K}^{(t)})} \right)}_{L_{v}^{(t-1)}} \\ &= \text{const.} + \mathbb{E}_{q} \left[\sum_{t=2}^{T} \sum_{v \in \mathcal{V}} \underbrace{D_{KL} \left(q(x_{v}^{(t-1)}|x_{v}^{(t)},x_{v}^{(0)}) \| p_{\theta}(x_{v}^{(t-1)}|\mathcal{G}_{v,K}^{(t-1)})} \right] - \sum_{v \in \mathcal{V}} \underbrace{\log p_{\theta}(x_{v}^{(0)}|\mathcal{G}_{v,K}^{(t)})}_{L_{v}^{(t-1)}} \right]}_{L_{v}^{(t)}} \\ &= \text{const.} + \mathbb{E}_{q} \left[\sum_{t=2}^{T} \underbrace{D_{KL} \left(q(x_{v}^{(t-1)}|x_{v}^{(t)},x_{v}^{(t)}) \| p_{\theta}(x_{v}^{(t-1)}|\mathcal{G}_{v,K}^{(t)})} \right)}_{L_{v}^{(t-1)}} \right] \\ &= \text{const.} + \mathbb{E}_{q} \left[\sum_{t=2}^{T$$

The advantage of this reformulation is that the forward process posteriors needed to compute the loss are tractable when conditioned on $x_v^{(0)}$:

$$q(\boldsymbol{x}_{v}^{(t-1)}|\boldsymbol{x}_{v}^{(t)}, \boldsymbol{x}_{v}^{(0)}) = \mathcal{N}(\boldsymbol{x}_{v}^{(t-1)}; \tilde{\boldsymbol{\mu}}_{t}(\boldsymbol{x}_{v}^{(t)}, \boldsymbol{x}_{v}^{(0)}), \tilde{\beta}_{t}\boldsymbol{I}), \tag{10}$$

with

$$\tilde{\boldsymbol{\mu}}_{t}(\boldsymbol{x}_{v}^{(t)}, \boldsymbol{x}_{v}^{(0)}) = \frac{1}{\sqrt{\alpha_{t}}} \left(\boldsymbol{x}_{v}^{(t)}(\boldsymbol{x}_{v}^{(0)}, \boldsymbol{\epsilon}) - \frac{\beta_{t}}{\sqrt{1 - \bar{\alpha}_{t}}} \boldsymbol{\epsilon} \right), \boldsymbol{\epsilon} \sim \mathcal{N}(\boldsymbol{0}, \boldsymbol{I})$$
(11)

and

$$\tilde{\beta}_t = \frac{1 - \bar{\alpha}_{t-1}}{1 - \bar{\alpha}_t} \beta_t \tag{12}$$

The term $L_v^{(t-1)}$, which is a KL divergence between two Gaussians, can now be written as:

$$L_{v}^{(t-1)} = \mathbb{E}_{q} \left[\frac{1}{2\sigma_{t}^{2}} \left\| \tilde{\boldsymbol{\mu}}_{t}(\boldsymbol{x}_{v}^{(t)}, \boldsymbol{x}_{v}^{(0)}) - \boldsymbol{\mu}_{\theta}(\mathcal{G}_{v,K}^{(t)}, t) \right\|^{2} \right] + \text{const.}$$

$$= \mathbb{E}_{q} \left[\frac{1}{2\sigma_{t}^{2}} \left\| \frac{1}{\sqrt{\alpha_{t}}} \left(\boldsymbol{x}_{v}^{(t)}(\boldsymbol{x}_{v}^{(0)}, \boldsymbol{\epsilon}_{v}) - \frac{\beta_{t}}{\sqrt{1 - \bar{\alpha}_{t}}} \boldsymbol{\epsilon}_{v} \right) - \boldsymbol{\mu}_{\theta}(\mathcal{G}_{v,K}^{(t)}, t) \right\|^{2} \right] + \text{const.}$$

$$(13)$$

This suggests a new parametrization of μ_{θ} , which predicts the noise instead:

$$\boldsymbol{\mu}_{\theta}(\mathcal{G}_{v,K}^{(t)}, t) = \frac{1}{\sqrt{\alpha_t}} \left(\boldsymbol{x}_v^{(t)} - \frac{\beta_t}{\sqrt{1 - \bar{\alpha}_t}} \boldsymbol{\epsilon}_{\theta}(\mathcal{G}_{v,K}^{(t)}, t) \right)$$
(14)

With this, $L_v^{(t-1)}$ is as follows:

$$L_v^{(t-1)} = \mathbb{E}_q \left[\frac{\beta_t^2}{2\sigma_t^2 \alpha_t (1 - \bar{\alpha}_t)} \left\| \boldsymbol{\epsilon}_v - \boldsymbol{\epsilon}_{\theta}(\mathcal{G}_{v,K}^{(t)}, t) \right\|^2 \right]$$
 (15)

Ho et al. [23] found that training works even better with a simplified objective that ignores the weighting term in $L_v^{(t-1)}$ and treats $L_v^{(0)}$ similarly to all $L_v^{(t-1)}$

$$L_{\text{simple}}(\theta) = \mathbb{E}_{t \sim U(\{1, \dots, T\}), v \sim U(\mathcal{V}), q} \left[\left\| \boldsymbol{\epsilon}_{v} - \boldsymbol{\epsilon}_{\theta} \left(\mathcal{G}_{v, K}^{(t)}, t \right) \right\|^{2} \right]$$
 (16)

Sampling from q requires sampling a set of noise vectors, one for each node in v's neighborhood: $\{\epsilon_{v'} \sim \mathcal{N}(\mathbf{0}, \mathbf{I}) \mid v' \in \mathcal{V}_{v,K}\}$, and computing the noisy features in $\mathcal{G}_{v,K}^{(t)}$. The final loss can be written as:

$$L_{\text{simple}}(\theta) = \mathbb{E}_{t \sim U(\{1, \dots, T\}), v \sim U(\mathcal{V}), \{\boldsymbol{\epsilon}_{v'} \sim \mathcal{N}(\mathbf{0}, \mathbf{I}) \mid v' \in \mathcal{V}_{v, K}\}} \left[\left\| \boldsymbol{\epsilon}_{v} - \boldsymbol{\epsilon}_{\theta} \left(\mathcal{G}_{v, K}^{(t)}, t \right) \right\|^{2} \right]$$
(17)

B Additional Method Details

B.1 Database Reconstruction from its Graph Representation

In Section 3.1, we presented the graph representation of the RDB that we use for generation. An important property of this representation is that it is invertible, i.e., one can reconstruct the RDB from its graph representation after generating the graph. One way to perform this reconstruction is as follows:

- 1. For each node type i, assign a unique primary key $p_v \in \{1, \dots, n_i\}$ to each node v of type i. Nodes of the same type should have different primary keys.
- 2. For each edge $(v_1, v_2) \in \mathcal{E}$, add primary key p_{v_2} to the set of foreign keys \mathcal{K}_{v_1} .
- 3. For each node type i, construct table $R^{(i)}$ by stacking rows of the form $(p_v, \mathcal{K}_v, \boldsymbol{x}_v)$ for every node $v \in \mathcal{V}^{(i)}$.

B.2 Gaussian Diffusion for Categorical Variables

In Section 3.4.1, we discussed that our diffusion model applies Gaussian diffusion both to categorical and numerical features by first mapping categorical variables to continuous space through label encoding. Specifically, given a categorical feature with n distinct values $\{c_1,\ldots,c_n\}$, we apply a label encoindg scheme $E:\{c_1,\ldots,c_n\}\to\{0,\ldots,n-1\}$ that maps each unique category c_i to a unique integer value. Note that this process is invertible, allowing us to map generated values back to the categorical space.

Training and Sampling Algorithms

Algorithm 1 Training

- 1: repeat
- Sample $v \sim \text{Uniform}(\mathcal{V})$
- $(\mathcal{V}_{v,K}, \mathcal{E}_{v,K}, \mathcal{X}_{v,K}^{(0)}) \leftarrow \text{SELECT}_K(v; \mathcal{V}, \mathcal{E}, \mathcal{X}^{(0)}) \quad \triangleright K \text{-hop neighborhood around node } v$ $\text{Sample } t \sim \text{Uniform}(\{1, \dots, T\})$ $\text{Sample } \{\boldsymbol{\epsilon}_{v'} \sim \mathcal{N}(\mathbf{0}, \boldsymbol{I}) \mid v' \in \mathcal{V}_{v,K}\}$ 3:

- $\mathcal{X}_{v,K}^{(t)} \leftarrow \{\sqrt{\bar{\alpha}_t} \boldsymbol{x}_{v'}^{(0)} + \sqrt{1 \bar{\alpha}_t} \boldsymbol{\epsilon}_{v'} \mid v' \in \mathcal{V}_{v,K}\}$
- $\hat{\epsilon}_v \leftarrow \epsilon_{\theta}(\underbrace{(\mathcal{V}_{v,K}, \mathcal{E}_{v,K}, \mathcal{X}_{v,K}^{(t)})}_{\mathcal{G}_{v,K}^{(t)}}, t)$ 7:
- Take gradient descent step on $\nabla_{\theta} \| \boldsymbol{\epsilon}_v \hat{\boldsymbol{\epsilon}}_v \|^2$ 8:
- 9: until converged

Algorithm 2 Sampling

- 1: $\mathcal{X}^{(T)} \leftarrow \{\boldsymbol{x}_{v}^{(T)} \sim \mathcal{N}(\boldsymbol{0}, \boldsymbol{I}) \mid v \in \mathcal{V}\}$ 2: **for** $t = T, \dots, 1$ **do** 3: $\mathcal{Z} \leftarrow \{\boldsymbol{z}_{v} \sim \mathcal{N}(\boldsymbol{0}, \boldsymbol{I}) \text{ if } t > 1, \text{ else } \boldsymbol{z}_{v} = \boldsymbol{0} \mid v \in \mathcal{V}\}$ 4: $\mathcal{X}^{(t-1)} \leftarrow \left\{\frac{1}{\sqrt{\alpha_{t}}} \left(\boldsymbol{x}_{v}^{(t)} \frac{\beta_{t}}{\sqrt{1-\bar{\alpha}_{t}}} \epsilon_{\theta} \left(\mathcal{G}_{v,K}^{(t)}, t\right)\right) + \sigma_{t} \boldsymbol{z}_{v} \mid v \in \mathcal{V}\right\}$
- 5: end for
- 6: return $\mathcal{X}^{(0)}$

Heterogeneous Message-Passing Graph Neural Networks

A common way to process graph-structured data with deep learning models is using Message-Passing Graph Neural Networks (MP-GNNs). Since we are dealing with heterogeneous graphs, we leverage a heterogeneous message passing formulation, which supports a wide range of GNN architectures. Let $(\mathcal{G},t) \in \mathbb{G} \times \mathbb{R}$ denote the input to ϵ_{θ} with $\mathcal{G} = (\mathcal{V}, \mathcal{E}, \mathcal{X})$. We define initial node embeddings as $h_v^0 = (x_v, t) \ \forall \ v \in \mathcal{V}$. One iteration of message passing consists of computing updated node embeddings $\{h_v^{l+1}\}_{v\in\mathcal{V}}$ from the embeddings at the previous iteration $\{h_v^l\}_{v\in\mathcal{V}}$.

Given a node v, let $\phi(v)$ denote its type in the graph and let E_v denote the set of distinct edge types adjacent to v. One iteration (or layer) of heterogeneous message passing updates v's embedding h_n^l as follows. First, a distinct message is computed for each edge type:

$$\forall e \in E_v, \ \boldsymbol{m}_{v,e}^{l+1} = \{ \{ g_e(\boldsymbol{h}_w^l) \mid w \in \mathcal{N}_e(v) \} \},$$

where $\mathcal{N}_e(v)$ is the e-specific neighborhood of node v. Then, these messages are combined into a single unified message:

$$\mathbf{m}_{v}^{l+1} = \{ f_{e}(\mathbf{m}_{v,e}^{l+1}) \mid e \in E_{v} \} ,$$

which is used to update the node embedding:

$$h_v^{l+1} = f_{\phi(v)}(h_v^l, m_v^{l+1}).$$

 g_e , f_e and $f_{\phi(v)}$ are arbitrary differentiable functions with learnable parameters and $\{\cdot\}$ is a permutation-invariant set aggregator such as mean, max, etc.. Different GNN architectures can be obtained through specific choices of these functions.

C Experimental Details

C.1 Datasets

	# TABLES	# FOREIGN KEY PAIRS	Dертн	TOTAL # ATTRIBUTES	# ROWS IN LARGEST TABLE
Berka	8	8	4	41	1,056,320
Intacart 05	6	6	3	12	1,616,315
RelBench-F1	9	13	3	21	28, 115
Movie Lens	7	6	2	14	996, 159
CCS	5	4	2	11	383, 282
California	2	1	2	15	1,690,642

Table 3: Dataset Specifics

C.2 Implementation Details

C.2.1 GRDM hyperparameters and training

Architecture. For the GNN, we use the heterogeneous version of the GraphSAGE model [29] with the number of layers set to the number of hops K from the diffusion model. In our experiments, we set K=2 for the more complex databases with depth more than 3, which are Berka, Instacart 05, and RelBench-F1, and K=1 for the simpler ones, which are California, MovieLens, and CCS. We use sum-base aggregation and a hidden dimension of 128 for the GNN.

For the MLP, we follow [15] and use the same architecture to ensure a fair comparison. The MLP has layer sizes 512, 1024, 1024, 1024, 1024, 512 and follows the TabDDPM implementation [8]. All input and output dimensions of the GNN and MLP are adapted to the data dimensions. We also incorporate timestep information by encoding timesteps into sinusoidal embeddings, which are then added to the data.

Diffusion hyperparameters. We also follow [15] and set the diffusion timesteps T=2000 and use cosine scheduler for the noise schedule.

Training hyperparemters. We also follow [15] and use the AdamW optimizer with learning rate 6e-4 and weight decay 1e-5. We use 100,000 training steps for California and 200,000 on all other databases. For our model, we use a smaller batch size of 1024 compared to all baselines, which use 4096, which effectively means our model does 4x fewer passes on the data.

C.2.2 Baselines

For all diffusion baselines, we use exactly the same set of hyperparameters, including diffusion timesteps, MLP architecture, and training. However, we train all baselines with a larger batch size for the same number of steps, which gives them an advantage over our model.

For SDV, we use the default setting of their HMASynthesizer, which by default uses a Gaussian Copula synthesizer.

C.2.3 Hardware

All experiments are run using a single NVIDIA GPU GeForce RTX 2080 Ti.

C.3 Detailed Metrics Computation

First, we define the distribution similarity measures that are used across the different metrics in this work.

For numerical variables, we use the complement of the Kolmogorov-Smirnov (KS) statistic. The KS statistic between two numerical distributions is defined as the maximum difference between their respective cumulative density functions (CDFs).

$$KS = \sup_{x} |F_{real}(x) - F_{syn}(x)|,$$

where F_{real} and F_{syn} denote the CDFs of the real and synthetic variables, respectively. We always report the scaled complement (1 - KS) * 100 such that a higher score means better quality.

For categorical variables, we use the complement of the Total Variation (TV) distance. The TV distance between two categorical distributions compares their probabilities as follows:

$$TV = \frac{1}{2} \sum_{\omega \in \Omega} |R_{\omega} - S_{\omega}|,$$

where Ω is the set of all categories, R_{ω} and S_{ω} are the real and synthetic probabilities for a category $\omega \in \Omega$. We always report the scaled complement (1 - TV) * 100 such that a higher score means better quality.

We now present how each metric is computed in detail.

Cardinality. For each parent-child pair in the database, we compute the cardinality of each parent row, i.e., the number of children that each parent row has. This defines a numerical distribution for the real and synthetic data, for which we compute the complement of the KS statistic. The cardinality score is then the average across all parent-child pairs in the database.

Column Shapes. For each column in every table of the database, we measure the similarity between the column's marginal distribution in the real and synthetic databases. For numerical values, we use the complement of the KS statistic, while for categorical values, we use the complement of the TV distance. The Column Shapes metric is the average across all columns in the database.

Intra-Table Trends. For each pair of columns within the same table, we compute different correlation metrics depending on whether the columns are numerical or categorical (for a pair of numerical and categorical columns, we first discretize the numerical column into bins, then treat both columns as categorical). The Intra-Table Trends is the average of the correlation scores across all column pairs from the same table in the database.

For a pair of numerical columns, A and B, we compute the Pearson correlation coefficient defined as

$$\rho_{A,B} = \frac{Cov(A,B)}{\sigma_A \sigma_B},$$

where Cov is the covariance, σ_A and σ_B are the standard deviations of A and B, respectively. We compute this metric for both the real and synthetic pair, yielding $R_{A,B}$ and $S_{A,B}$, respectively. We

report the normalized score
$$\left(1 - \frac{\left|S_{A,B} - R_{A,B}\right|}{2}\right) * 100$$

For a pair of categorical columns, A and B, we compute the normalized contingency table, which consists of the proportion of rows that have each combination of categories in A and B, i.e., how often each pair of categories co-occur in the same row. We compute this matrix on both the real and synthetic pairs, yielding $R_{A,B}$ and $S_{A,B}$, respectively. We then compute the difference between them using the TV distance as follows:

$$score = \frac{1}{2} \sum_{\alpha \in \Omega_A} \sum_{\beta \in \Omega_B} |S_{A,B}(\alpha,\beta) - R_{A,B}(\alpha,\beta)|,$$

where Ω_A and Ω_B are the set of possible categories of columns A and B, respectively. We again report the normalized score (1 - score) * 100.

Inter-Table Trends (k-hop). This metric is similar to the Column Pair Trends, but instead of computing the correlation on column pairs from the same table, it computes it on column pairs from tables that are within k hops from each other. For example, 1-hop considers all parent-child pairs, 2-hop considers a column in some table and its correlation with columns from its parent's parent or child's child, etc. For every possible hop k, we report the average across all possible pairs. In practice, this is implemented by denormalizing the pair of tables into a single one and then computing the Column Pair Trends metric.